

# Engineering Photosystem I Complexes with Metal Oxide Binding Peptides for Bioelectronic Applications

Richard F. Simmerman,<sup>†</sup> Tuo Zhu,<sup>†</sup> David R. Baker,<sup>‡</sup> Lijia Wang,<sup>§</sup> Sanjay R. Mishra,<sup>§</sup> Cynthia A. Lundgren,<sup>‡</sup> and Barry D. Bruce<sup>\*,†</sup>

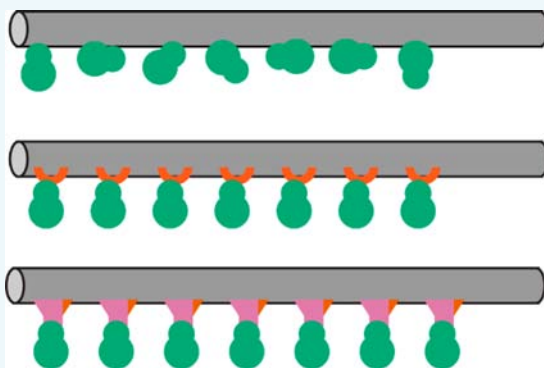
<sup>†</sup>Department of Biochemistry and Cellular and Molecular Biology, University of Tennessee Knoxville, Knoxville, Tennessee 37919, United States

<sup>‡</sup>Sensors and Electron Devices Directorate, U.S. Army Research Laboratory, Adelphi, Maryland 20783, United States

<sup>§</sup>Department of Physics, University of Memphis, Memphis, Tennessee 38152, United States

## S Supporting Information

**ABSTRACT:** Conventional dye-sensitized solar cells comprise semi-conducting anodes sensitized with complex synthetic organometallic dyes, a platinum counter electrode, and a liquid electrolyte. This work focuses on replacing synthetic dyes with a naturally occurring biological pigment–protein complex known as Photosystem I (PSI). Specifically, ZnO binding peptides (ZOBiP)-fused PSI subunits (ZOBiP–PsaD and ZOBiP–PsaE) and TiO<sub>2</sub> binding peptides (TOBiP)-fused ferredoxin (TOBiP–Fd) have been produced recombinantly from *Escherichia coli*. The MOBiP-fused peptides have been characterized via western blotting, circular dichroism, MALDI-TOF, and cyclic voltammetry. ZOBiP–PSI subunits have been used to replace wild-type PsaD and PsaE, and TOBiP–Fd has been chemically cross-linked to the stromal hump of PSI. These MOBiP peptides and MOBiP–PSI complexes have been produced and incubated with various metal oxide nanoparticles, showing increased binding when compared to that of wild-type PSI complexes.



## INTRODUCTION

Cyanobacteria, algae, and plants harvest solar energy via oxygenic photosynthesis in order to convert and store chemical energy.<sup>1</sup> Two photosynthetic reaction centers, Photosystem II (PSII) and Photosystem I (PSI), residing in the thylakoid membranes of these organisms, are responsible for photo-induced charge separation events.<sup>2</sup> While both of these multi-subunit-containing, membrane-bound photosystems have been incorporated into photovoltaic devices<sup>3</sup> and hydrogen-producing devices,<sup>4,5</sup> PSI has several key advantages for its use in biohybrid solar energy-harvesting devices. These include an extremely long functional lifetime,<sup>6</sup> a more negative reducing potential than that of PSII,<sup>7</sup> placement of electron transfer cofactors, F<sub>A</sub> and F<sub>B</sub>, outside of the hydrophobic bilayer, and the ability to specifically donate electrons to soluble acceptors ferredoxin (Fd) and flavodoxin.<sup>8</sup>

Because of these advantages, the goal of this work is to enhance the surface selectivity of PSI through the use of binding peptides. However, a challenge that must be overcome with wild-type PSI is that, when employed in a photovoltaic device, it can adsorb to an electrode in a variety of configurations, including nonproductively and even counter productively, as shown in Figure 1a. Different metal oxide binding peptides (MOBiP) identified and shown by phage display to selectively bind either ZnO<sup>9</sup> or TiO<sub>2</sub><sup>10</sup> were

engineered onto stromal subunits of PSI or Fd, respectively. We hypothesize that these ZnO and TiO<sub>2</sub> binding peptides (ZOBiPs/TOBiPs) will be able to increase binding efficiency and confer a uniform, productive directionality to the binding of PSI complexes onto these metal oxide semiconductors (Figure 1b). The semiconductors ZnO and TiO<sub>2</sub> were chosen because of their relatively high abundance, stability, and lack of toxicity.<sup>11</sup> These metal oxides and MOBiP–PSI complexes will eventually be used to create biohybrid dye-sensitized solar cells (BH-DSSCs).

While the efficiency of traditional DSSCs, which use ruthenium-based dyes to absorb photons and inject electrons into a semiconductor (Figure 2a), has climbed to over 13%,<sup>12</sup> there are still some limitations with this type of DSSC. These include the lack of availability of the dye and platinum, which is typically used as a counter electrode, the stability of the dye, and the toxicity of the electrolyte solution.<sup>13</sup> It is these limitations that PSI-based BH-DSSCs (Figure 2b) can help to overcome. While most proteins are not stable for extended periods of time, PSI has been shown to retain function in

Received: July 6, 2015

Revised: August 17, 2015

Published: August 24, 2015



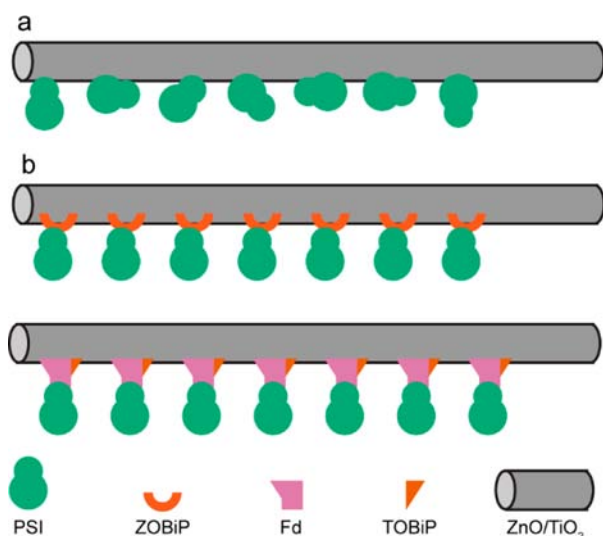


**Figure 1.** MOBiP–PSI complexes productively bind to metal oxides. (a) PSI binding to a metal oxide semiconductor in a variety of conformations, including productive, nonproductive, and counterproductive. (b) ZOBiP–PSI or TOBiP–Fd–PSI complex binding to a metal oxide semiconductor in uniformly productive conformations.

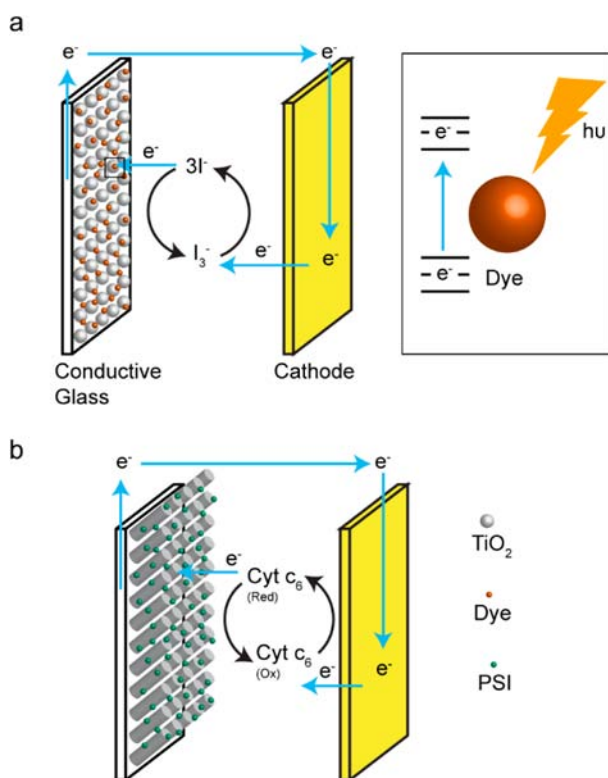


**Figure 2.** Traditional and bio-hybrid dye-sensitized solar cells. (a) Traditional DSSC with synthetic dye,  $\text{TiO}_2$  semiconductor, conductive glass, and liquid electrolyte  $3\text{I}^-/\text{I}_3^-$ . (b) BH-DSSC with PSI instead of a synthetic dye and  $\text{TiO}_2$  nanowires to increase surface area. The native electron donor to PSI, Cyt  $c_6$ , functions as the electrolyte.

photochemical cells for months, even after evaporation and resuspension in the electrolyte solution.<sup>6</sup>

Although many scientists conclude that the proteinaceous basis of PSI would render it labile and limit its functional half-life, work in our lab and others has clearly shown that isolated PSI from cyanobacteria and plants can function to produce

hydrogen or photocurrent for greater than 80<sup>5</sup> and 280 days,<sup>6</sup> respectively. Moreover, we have also made some rough calculations to show that, using existing isolation methods, an acre of spinach could sustainably yield enough PSI to produce very large levels of hydrogen<sup>5</sup> and >40 acres of PSI-based solar cells<sup>3</sup> photocurrents. It has been estimated that even by using bench-scale production methods the materials required to fabricate PSI-based solar cells could be ~10 cents per  $\text{cm}^2$  of active electrode area.<sup>6</sup>

This article details bioengineering methods and reagents required to accomplish the goal of fabricating MOBiP–PSI complexes. First, recombinant ZOBiP–PSI stromal subunits PsaD and PsaE (Figure 3a) along with TOBiP–Fd (Figure 3b)

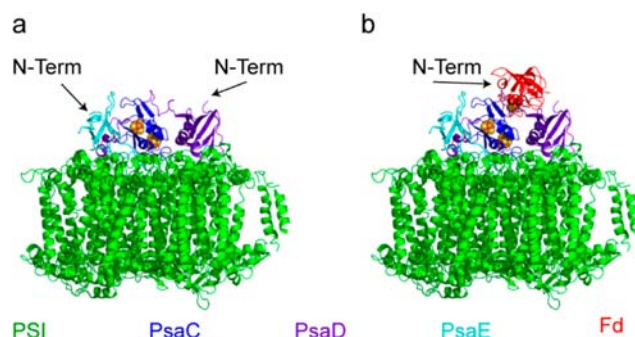


**Figure 3.** Accessibility of the N-termini of PsaD, PsaE, and Fd. (a) PSI with the stromal hump highlighted. The  $[4\text{Fe}-4\text{S}]$  centers,  $F_A$  and  $F_B$ , of PsaC are shown in space-filling representation in yellow and orange (PDB ID 1JBO). (b) PSI–Fd (PDB ID 2CJN) model from previous work.<sup>15</sup>

were produced and purified. These modified subunits were then characterized by mass spectrometry and difference spectroscopy. Then, wild-type (WT) PsaD and PsaE incorporated in isolated PSI were replaced with ZOBiP–PsaD and ZOBiP–PsaE, and TOBiP–Fd was cross-linked to WT PSI to create MOBiP–PSI complexes.

The binding of these MOBiP–PSI complexes to their respective metal oxides was also examined, and cyclic voltammetry (CV) was employed to ensure that the addition of the MOBiPs did not interfere with the abilities of the proteins to donate or accept electrons.

## RESULTS AND DISCUSSION

### Engineering MOBiPs onto Photosynthetic Proteins.

In the search for a mechanism that would allow PSI complexes to specifically and preferentially bind  $\text{ZnO}$  and  $\text{TiO}_2$ , peptides that had been selected for their abilities to do just that via phage display were selected.<sup>9,10</sup> These MOBiPs are highly specific, for example, ZOBiP will not bind cadmium oxide,<sup>8</sup> but it binds to  $\text{ZnO}$  very well, with 3 to 4 bacteria observed to interact with each  $\text{ZnO}$  particle. The high-resolution crystal structure of PSI<sup>14</sup> allowed for a design in which the ZOBiP stromal subunits were fused onto the N-termini of PsaD and PsaE to lessen the chance of interference with PSI assembly. No such crystal structure is available for the PSI–Fd complex. This was addressed in previous work using the principles of protein frustration, where it was determined that the N-terminus of Fd is less likely to be involved in the docking of Fd–PSI;<sup>15</sup> thus, TOBiP was fused onto the N-terminus of Fd.

**Production and Purification of ZOBiP–PsaD/E and TOBiP–Fd.** MOBiPs were added onto the N-termini of PSI

subunits and Fd via DNA primers (Integrated DNA Technologies). ZOBiP-PSI and TOBiP-Fd were then cloned into the pTYB2 vector (Invitrogen). This construct takes advantage of a thiol-induced cleavage to produce a tagless protein. The MOBiP-containing and WT proteins were recombinantly produced in *Escherichia coli* (Figure 4a), and purified WT subunits and Fd were lyophilized and used to generate polyclonal antibodies.

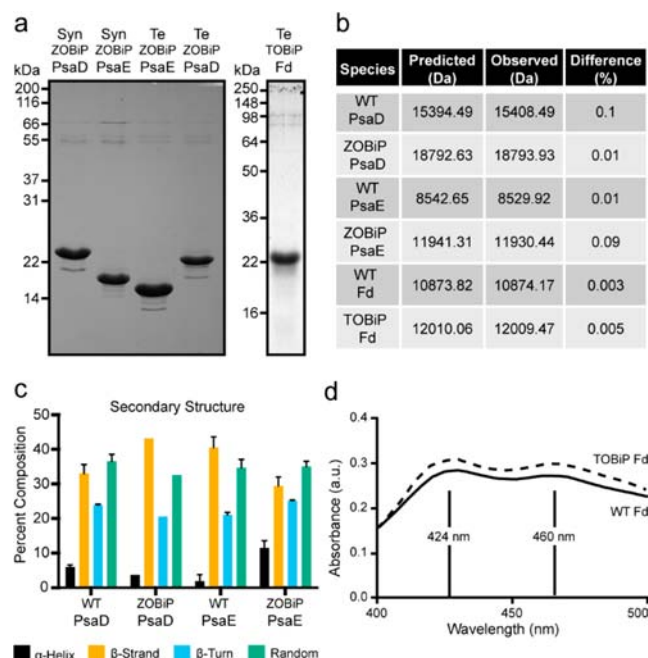


**Figure 4.** Confirmation of recombinant MOBiP peptides. (a) SDS-PAGE showing production and purity of ZOBiP-PsaE, ZOBiP-PsaD, and TOBiP-Fd. (b) Results from MALDI-TOF with the predicted and observed molecular weights of recombinant WT/MOBiP peptides. (c) Deconvoluted CD spectra showing the secondary structure of the WT/ZOBiP-PSI subunits. (d) Characteristic difference in absorbance spectrum of reduced-oxidized species of WT/TOBiP Fd.

**Characterization of MOBiP Peptides.** After expression and purification of the ZOBiP-PSI subunits and TOBiP-Fd, the peptides were assayed to ensure that the metal oxide binding peptides did not interfere with their structure and function. Matrix-assisted laser desorption/ionization time-of-flight (MALDI-TOF) mass spectrometry (MS) was used to confirm the primary structure of the WT and MOBiP proteins (Figure 4b). Circular dichroism (CD) was then performed on WT PsaD/E, ZOBiP-PsaD/E, WT-Fd, and TOBiP-Fd to confirm that the secondary structure of PsaD was not altered by the N-terminal addition of MOBiP (Figure 4c). The addition of ZOBiP to PsaE seems to confer some extra alpha-helical content to the subunit. This could be due to the fact that PsaE is not complexed with the rest of PSI and its secondary structure is more easily perturbed as a solitary soluble peptide. The results indicated that the introduction of the MOBiPs did not perturb the secondary structure of PsaD, PsaE, or Fd. The absorbance spectra of functional Fd differs at 330, 424, and 460 nm, depending on the redox state of the molecule.<sup>16</sup> Taking the difference of the oxidized minus reduced states yields a characteristic spectrum that demonstrates that Fd is functional (i.e., it can both accept and donate electrons).<sup>16</sup> The addition of

the TOBiP to the Fd did not alter this characteristic oxidized minus reduced spectrum, suggesting that neither the native structure nor the function of the Fd was altered by the fusion of TOBiP (Figure 4d).

**Optimizing Binding of MOBiP Peptides to Metal Oxides.** After confirmation of the primary structure, secondary structure, and functionality of the MOBiP peptides, the ability of MOBiPs to enhance binding of the fusion protein relative to that of wild type was investigated. Different TiO<sub>2</sub> binding peptides (Figure 5a), nanoparticles (NPs) (Figure 5b), buffer pH values (Figure 5c), and additives (Supporting Information Figure S2) were used to discover conditions that optimized binding of TOBiP-Fd. The different NPs were examined with SEM (Supporting Information Figure S2). The best binding

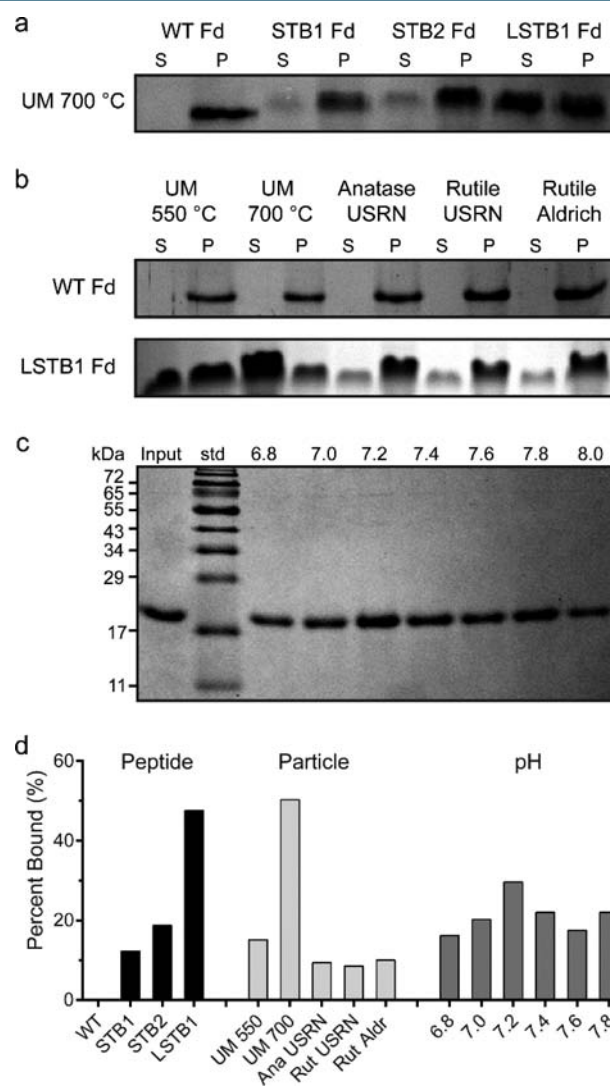


**Figure 5.** Optimizing affinity of TOBiP-Fd for TiO<sub>2</sub>. (a) SDS-PAGE with TOBiP-Fd in the supernatant [S] and pellet [P] of WT-Fd and three different TOBiP-Fds incubated with TiO<sub>2</sub> from the University of Memphis 700 °C. (b) SDS-PAGE with TOBiP-Fd in S and P of LSTB1 TOBiP-Fd incubated with TiO<sub>2</sub> from the University of Memphis 700 °C, University of Memphis 550 °C, Anatase TiO<sub>2</sub> from US research nanomaterials, Rutile TiO<sub>2</sub> from US research nanomaterials, and Rutile TiO<sub>2</sub> from Aldrich. (c) SDS-PAGE of LSTB1-TOBiP-Fd in pellet with TiO<sub>2</sub> from the University of Memphis 700 °C in 0.1× PBS at various pH. (d) SDS-PAGE data from A–C quantified by ImageJ.



was observed in 0.1× PBS, pH 7.2, with 3% (v/v) DMSO using nanospheres (NS) manufactured at the University of Memphis (Figure 5d). Experiments were performed by incubating protein with metal oxide NPs and then separating the NPs via centrifugation. The pellets were washed, and then protein was eluted from the metal oxide by boiling with Laemmli sample buffer. This was also repeated for ZOBiP–PsaD/E, but none of the conditions tested resulted in better binding of ZOBiP–PsaD/E than WT PsaD/E to ZnO (results not shown). We hypothesized that this may not matter, as the assay was attempted with soluble PsaD/E that would be far more accessible than PsaD/E incorporated into PSI. The test was performed later with ZOBiP–PsaD/E incorporated PSI. The NSs (in particular, the 700 °C calcined sample) from the University of Memphis were the best at TiO<sub>2</sub> retention. This could be explained by their smaller size, meaning that their surface area to volume ratio would be the highest.

**Replacing PsaD/E with ZOBiP–PsaD/E.** It has previously been shown that stromal subunits PsaD and PsaE are assembled into PSI in the thylakoid membranes without the need for ATP or stromal fraction<sup>17</sup> and that recombinant PsaD and PsaE can replace their corresponding subunits in isolated PSI<sup>17,18</sup> (Figure 6a). This has been accomplished with ZOBiP–

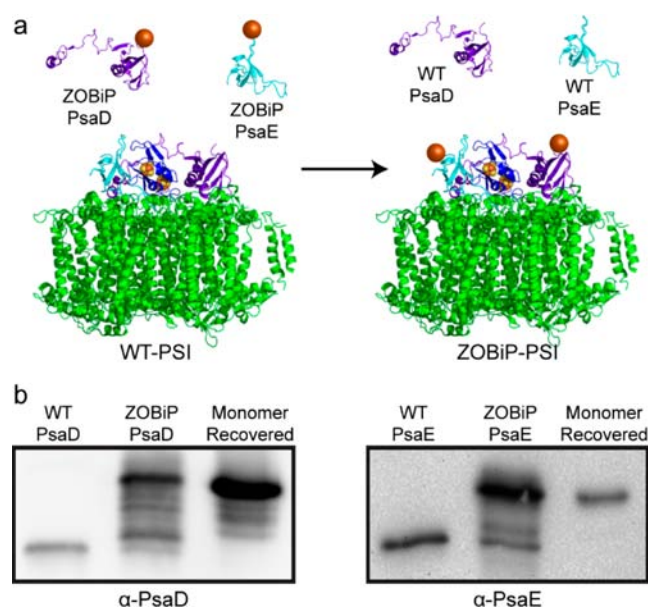


**Figure 6.** Replacement of WT PSI subunits with ZOBiP–PsaD/E. (a) Replacement of PsaD/PsaE in WT PSI by incubation with ZOBiP–PsaD/E. (b) Western blot of WT PsaD/E, ZOBiP–PsaD/E, and ZOBiP–PsaD/E replaced PSI after recovery of PSI.

PsaE;<sup>19</sup> however, the ZOBiP–PsaE from that work is from *M. laminosa* and incorporated into PSI from *Thermosynechococcus elongatus*. In the present work, ZOBiP–PsaD and ZOBiP–PsaE are from the same organism as that from which PSI was harvested, either *T. elongatus* (T.e.) or *Synechocystis* 6803 (Syn 6803). This should allow for a more complete replacement of WT PsaD/E and result in a more functionally active ZOBiP–PSI. This was accomplished very well (nearly 100% exchange) for Syn 6803, and nearly 50% exchange was observed for T.e., as quantified via western blotting (Figure 6b). Replacement reactions were performed at 20 °C, which is very close to the temperature at which Syn 6803 grows, but it is roughly 30 °C colder than that at which T.e. lives. We believe that a

replacement reaction for T.e. performed at 55 °C, the temperature at which T.e. PSI naturally assembles, would result in much better replacement. All PSI complexes were recovered via ultracentrifugation over a continuous sucrose gradient.

**Formation of TOBiP–Fd–PSI Complexes.** ZOBiP–PSI complexes were formed via replacement of WT PsaD/E with ZOBiP–PsaD/E. Another goal of this work is to form TOBiP–Fd–PSI complexes because Fd is the natural electron acceptor of PSI.<sup>8</sup> The N-terminus of Fd has been modified via addition of TOBiP to enhance binding to TiO<sub>2</sub>.<sup>15</sup> Incorporation of Fd into a MOBiP–PSI complex could drastically decrease the chances of charge recombination by separating the electron even farther from the hole left in P<sub>700</sub><sup>+</sup>. Both WT and TOBiP–Fd were chemically cross-linked to purified PSI (Figure 7).

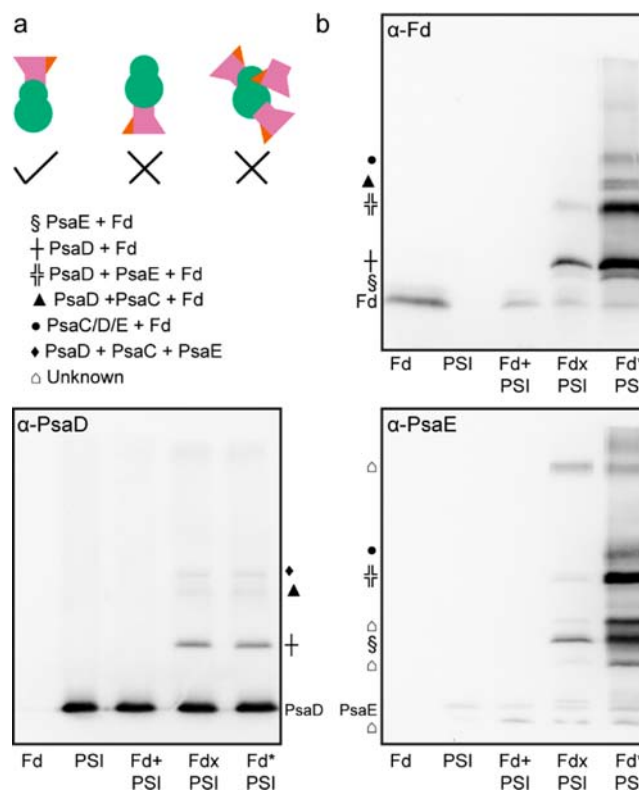


**Figure 7.** Cross-linking to produce PSI–Fd heterodimer. (a) Scheme of PSI–Fd species that is desired. (b) Western blots of the cross-linking reactions with α-PsaD, α-PsaE, and α-Fd antibodies. The FdxPSI reaction produced species consistent with a PSI–Fd heterodimer. Fd + PSI reaction was performed at 4 °C for 5 s, FdxPSI was performed at room temperature for 5 s, and Fd\*PSI was performed at room temperature for 30 s.

These reactions were optimized to maximize the yield of a final product that coincided with a Fd–PSI heterodimer while attempting to minimize nonspecific cross-linked products (Figure 7a). All PSI complexes were recovered via ultracentrifugation over a continuous sucrose gradient. The results from the various PSI–Fd cross-linking reactions were run on SDS-PAGE gels and verified by western blotting with the antibodies that were produced earlier (Figure 7b). The results from cross-linking PSI with WT Fd were compared to the results from cross-linking PSI with TOBiP–Fd (Figure 7c). Because there was negligible difference in the western blots (besides a small size shift attributed to the increased size of

TOBiP–Fd), the hypothesis that the TOBiP itself had no effect on the interaction between Fd and PSI was corroborated.

**Binding of PSI Complexes to Metal Oxides Is Enhanced by Inclusion of MOBiPs.** Because the ZOBiP did not increase binding of soluble PsaD/E compared to that of wild type, the same binding assay was performed on PSI that had undergone the exchange reaction with either ZOBiP–PsaD/E or WT PsaD/E. The exchanged PSI complexes were recovered via ultracentrifugation over a continuous sucrose gradient. WT and ZOBiP PSI were then allowed to bind with ZnO NPs (US Research Nanomaterials). Samples of the unbound, washed, and bound PSI were quantitated via chlorophyll a absorbance in Figure 8a. This showed that

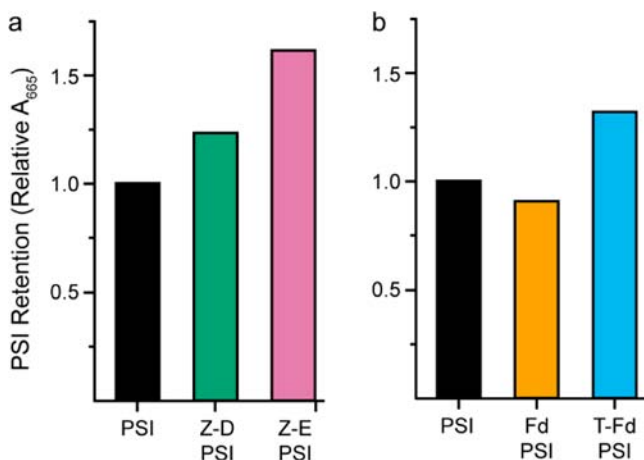


**Figure 8.** MOBiPs enhance binding of PSI complexes. (a) Amount of WT-PSI, ZOBiP–PsaD–PSI, and ZOBiP–PsaE–PSI bound to NPs of ZnO. (b) Amount of PSI cross-linked alone, to WT Fd, or to TOBiP–Fd bound to NSs of TiO<sub>2</sub>. WT-PSI bound to the particle is standardized to 1.

ZOBiP–PsaD–PSI binds ~20% better than WT-PSI and that ZOBiP–PsaE–PSI binds ~60% better. This will be advantageous because it means that a higher concentration of PSI may be used in BH-DSSCs that incorporate these PSI complexes. The larger increase of PSI bound by ZOBiP–PsaE–PSI may be the result of PsaE being more flexible than PsaD in the PSI complex, as can be seen by the more than 60% random coil that PsaE adopts in a crystal structure.<sup>14</sup> This could allow PsaE to move and more effectively bridge the gap between the stromal hump of PSI and the ZnO nanoparticle. These experiments were performed only once; although the numerical values of the gains that the MOBiPs provide are not certain, we believe that the MOBiPs will enhance binding.

PSI–Fd complexes (both WT Fd and TOBiP–Fd) generated above were also tested for their ability to bind TiO<sub>2</sub>. As shown in Figure 8b, the cross-linking of PSI–Fd decreases the amount of protein retained by the TiO<sub>2</sub> NSs when compared to that of PSI alone by ~10%. However, PSI–TOBiP–Fd binds TiO<sub>2</sub> 45% better than PSI–Fd and 30% better than PSI alone. This means that not only can more PSI be deposited when conjugated to TOBiP–Fd but also that it is likely directionally oriented. This may allow for the creation of BH-DSSCs with the vast majority of PSI complexes in a position to productively contribute to photocurrent generation.

**Redox Potentials of Fd and PSI Not Altered by MOBiPs.** WT–Fd and TOBiP–Fd were adsorbed to TiO<sub>2</sub>-sintered ITO glass slides, and WT–PSI and ZOBiP–PSI were

adsorbed to ZnO-sintered ITO glass slides. Cyclic voltammetry was used to evaluate the midpoint potentials of these species and whether the inclusion of TOBiP or ZOBiP had any effect on the electrochemical properties of the proteins. The resulting voltammograms show WT–PSI and ZOBiP–PSI (Figure 9a)

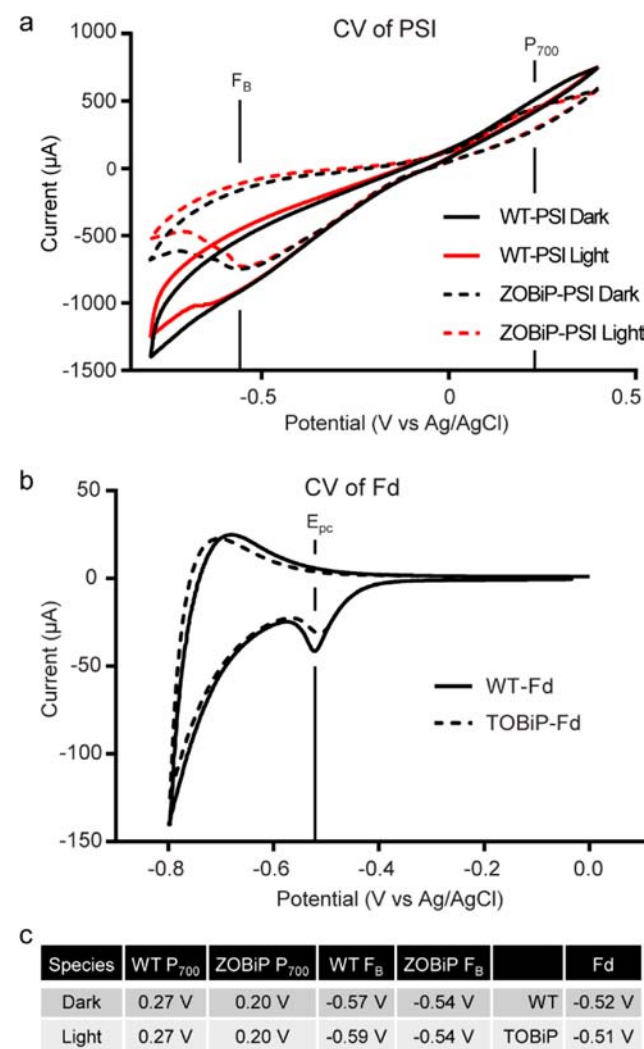


**Figure 9.** MOBiPs do not alter electrochemical properties of proteins. (a) Cyclic voltammetry of WT–PSI and ZOBiP–PSI. (b) Cyclic voltammetry of WT–Fd and TOBiP–Fd. (c) Midpoint potentials are unchanged by the addition of the MOBiPs.

along with WT–Fd and TOBiP–Fd (Figure 9b). The midpoint potentials for F<sub>B</sub> and P<sub>700</sub> of PSI (Figure 9a) and the [2Fe–2S] of Fd (Figure 9b) are highlighted on the figures and reported in Figure 9c. The voltammograms demonstrate that the addition of the MOBiPs does not alter the abilities of the proteins to donate and receive electrons or the midpoint potential of any of the protein complexes.

In conclusion, we have incorporated a functional ZOBiP and TOBiP onto the N-termini of PsaD/E and Fd, respectively. These fusion peptides were produced recombinantly in *E. coli* (Figure 4a) and have been confirmed via MALDI-TOF (Figure 4b), CD (Figure 4c), and an altered absorbance spectrum (Figure 4d). MOBiP–PSI complexes have been assembled using ZOBiP–PsaD/E to form ZOBiP–PSI (Figure 5) and using TOBiP–Fd via cross-linking to form TOBiP–Fd–PSI (Figure 6). These MOBiP–PSI complexes have been shown to

have increased binding to their appropriate metal oxide (Figure 7). Cyclic voltammetry has shown that the addition of the MOBiPs does not alter the midpoint potential of the proteins or their ability to donate and accept electrons. This will allow for increased amounts of PSI to be captured by the metal oxide semiconductors for incorporation into BH-DSSCs. Because more protein is bound due to the MOBiP, it is reasonable to speculate that MOBiP–PSI is orientated with the MOBiP toward its corresponding metal oxide. The distance between the final electron acceptor in the MOBiP–PSI complex and the semiconductor may be reduced to a point that a soluble redox carrier will not be necessary to facilitate electron transfer. Production and incorporation of these MOBiP–PSI complexes into electrophotocatalytic cells may allow for increases in photocurrent production in BH-DSSCs. This would represent a type of semiconductor–photosynthetic-protein hybrid that has been reviewed in ref 20. Future work will investigate the utility of these constructs in biohybrid solar cells.

## ■ EXPERIMENTAL PROCEDURES

**General Experimental.** Reagents and solvents were generally purchased from Aldrich, Gold Biotechnology, or Fisher Scientific and used as received. Dodecyl- $\beta$ -D-maltopyranoside ( $\beta$ -DM) was purchased from Glycon Biochemicals GmbH.

**Purification of PSI.** Photosystem I was purified from T.e. and Syn 6803 in an identical manner, which was performed similarly to that in ref 5. Frozen cells were resuspended in 30 mL of ice-cold lysozyme buffer (50 mM HEPES, pH 8.0, 500 mM sorbitol, 10 mM  $\text{CaCl}_2$ , 10 mM  $\text{MgCl}_2$ ) and homogenized in a dounce homogenizer. The chlorophyll concentration of the solution was then measured spectrophotometrically. The cells were then centrifuged at 5000g for 10 min at 4 °C. The pellet was then resuspended in ice-cold lysozyme buffer at a concentration of 1 mg/mL chlorophyll. Lysozyme was then added to a final concentration of 0.25% (w/v), and the cells were then incubated in the dark at 37 °C for 45 min. The cells were then centrifuged at 5000g for 10 min at 4 °C. The supernatant was discarded, and the cells were resuspended at 1 mg/mL chlorophyll in lysis buffer (20 mM MES, pH 6.4, 10 mM  $\text{CaCl}_2$ , 10 mM  $\text{MgCl}_2$ , 500 mM sorbitol). Cells were then lysed via three passes through the French Press at an internal pressure of 25 000 psi. The lysate was then centrifuged at 35 000g for 30 min at 4 °C. The pellet was resuspended in wash buffer (20 mM MES, pH 6.4, 10 mM  $\text{CaCl}_2$ , 10 mM  $\text{MgCl}_2$ ), homogenized, and spun again. The pellet was then resuspended at 2 mg/mL chlorophyll in wash buffer supplemented with 3 M NaBr, homogenized, diluted to 1 mg/mL chlorophyll with wash buffer, and centrifuged as above. The pellet was then resuspended at 1 mg/mL in wash buffer, homogenized, and spun again.

The protein incorporated in the washed membranes was then solubilized. The pellet was resuspended to 1.06 mg/mL chlorophyll, and  $\beta$ -DM was added to a final concentration of 0.6% (w/v) from a 10% (w/v) stock. The membranes were then incubated at 20 °C for 30 min with gentle shaking. The membranes were centrifuged at 35 000g for 20 min, and the supernatant was gently loaded on top of sucrose gradients using around 4 mL of solubilized membrane proteins per gradient. The gradients were centrifuged in a swinging bucket rotor at 100 000g at  $r_{\text{max}}$  for at least 12 h. The lower green band was recovered, dialyzed against 1 $\times$  wash buffer, resuspended to 1 mg/mL chlorophyll, and stored at –20 °C indefinitely.

**Generation of WT *PsaD* and *PsaE*.** Primers introducing an NdeI (CAT ATG) restriction site 5' and an XmaI (CCC GGG) restriction site 3' onto *psaD* and *psaE* from Syn 6803 and T.e. were designed. Primers were synthesized by Integrated DNA Technologies, received as a lyophilized powder, and resuspended to 50  $\mu\text{M}$  in  $\text{ddH}_2\text{O}$ . This constituted a 5 $\times$  stock, which was aliquoted and kept frozen at –20 °C. Working stocks of primers were made by diluting the 5 $\times$  stocks to 10  $\mu\text{M}$  to keep the 5 $\times$  stocks from contamination. PCR was performed with high-fidelity ExTaq DNA polymerase (Takara Bio Inc.). PCR was performed in a Mastercycler gradient cycler (Eppendorf).

The PCR product was run on a 0.8% agarose gel and purified using the Wizard SV Gel and PCR clean-up system (Promega). Purified PCR product was then ligated into the pGEM-T Easy vector (Promega). The product of the ligation was transformed into *E. coli* GC5 competent cells (Genesee Scientific) and spread onto 1.5% Luria broth (LB) agar plates containing 150  $\mu\text{g}/\text{mL}$  ampicillin.

Colony PCR products were run on a 0.8% agarose gel and visually inspected to confirm that an insertion corresponding with the desired product occurred. A positive colony was sequence-verified and grown overnight in LB with 150  $\mu\text{g}/\text{mL}$  ampicillin. A miniprep (Qiagen) was performed to isolate the pGEM-T Easy PSI-Subunit plasmid. DNA was quantified using  $A_{280}$  measured on a NanoDrop 3000 spectrophotometer (Thermo Scientific), aliquoted, and stored at –20 °C.

The pGEM-T Easy PSI subunit vectors along with the pTYB2 vector (New England Biolabs) were digested with NdeI and XmaI for 90 min at 37 °C, and enzymes were heat-killed at 65 °C for 20 min. The digested pTYB2 vector was incubated with 1  $\mu\text{L}$  of calf intestine alkaline phosphatase (CIAP, Promega) for 1 h at 37 °C to remove phosphate overhangs, inhibiting self-ligation. Digested PSI-subunit and CIAP-treated pTYB2 were run on a 0.8% agarose gel and purified using the Wizard SV Gel and PCR clean-up system. The purified insert and vector were ligated for 2 h at 25 °C. The ligation products were transformed into GC5 competent cells and plated onto 1.5% LB agar plates with 150  $\mu\text{g}/\text{mL}$  ampicillin. A positive colony was selected and grown overnight at 37 °C with shaking at 225 rpm in LB with 150  $\mu\text{g}/\text{mL}$  ampicillin, and a miniprep was performed to isolate the plasmid DNA. The plasmids were quantified, aliquoted, and frozen.

**Introduction of ZOBiP onto PSI Subunits.** The ZOBiP (zinc oxide binding peptide) is a 25-residue peptide<sup>9</sup> with a 3-glycine linker that is introduced onto the N-terminus of *PsaD* and *PsaE*. Primers coding for expression of this peptide were ordered with a 5' NdeI cleavage site and a 3' NotI cleavage site. Because of the reduction of price, four shorter primers with overlaps, instead of two, were purchased. Primers introducing a NotI site 5' of the *PsaD*/*PsaE* start codons were designed and purchased. This allowed us to make NdeI–NotI–PSI subunit–XmaI DNA via PCR. These were produced and ligated into pGEM-T Easy for 2 h at room temperature. The four primers used to make ZOBiP were resuspended to 1 mM with 1 $\times$  TE buffer. Five microliters of each ZOBiP primer was mixed and incubated at 95 °C for 2 min, room temp for 5 min, and 65 °C for 3 min three times and ligated into the pGEM–NdeI–NotI–PSI subunit–XmaI vector that was double-digested with NdeI and NotI for 2 h at room temperature. Two microliters of these reactions was transformed into competent GC10 *E. coli* cells and plated on 1.5% LB agar plates with 100  $\mu\text{L}/\text{mg}$  ampicillin. Insertion was verified via colony PCR.



**Production of Antibodies.** Polyclonal antibodies against recombinant Te-PsaD, Syn-PsaE, Te-PsaE, and Te-Fd were generated in rabbits by Pocono Rabbit Farm (Canadensis, PA) from lyophilized protein purified. Two rabbits were used to generate antibodies for each antigen, and the final bleed was compared to the serum isolated from the rabbits before they were injected with the antigen to determine which antibody was most suitable for use.

**Circular Dichroism Spectroscopy.** The secondary structure of the PSI subunits, with and without ZOBiP, was investigated using an Aviv series 202 circular dichroism (CD) spectrophotometer (Aviv Instruments). All purified subunits were brought to a concentration of 10  $\mu$ M and extensively dialyzed into 1 $\times$  CD buffer (10 mM potassium phosphate, pH 7.0, 50 mM Na<sub>2</sub>SO<sub>4</sub>). CD spectra for Syn PsaD, Syn PsaE, Syn ZOBiP–PsaD, Syn ZOBiP–PsaE, T.e. PsaD, T.e. PsaE, T.e. ZOBiP–PsaD, and T.e. ZOBiP–PsaE were generated at 25 °C from 285 to 185 nm with sampling at 1 nm intervals for 5 s. For each subunit, three independent scans were averaged, corrected for buffer contribution (also the average of 3 scans), smoothed, and converted to molar ellipticity using the Aviv software, version 3.37 MX. Deconvolution was performed using CDPPro software with IBase37, a reference set of 37 soluble proteins,<sup>21</sup> to determine the probable secondary structures of the PSI subunits. CDPPro uses three algorithms to deconvolute measured secondary structure: self-consistent method for CD analysis, version 3 (Selcon3<sup>22</sup>), Contin/LL,<sup>23</sup> and CDSSTR.<sup>24</sup>

**MALDI-TOF of PSI Subunits.** Wild-type and ZOBiP-containing PsaD/E were analyzed by matrix-assisted laser desorption ionization time-of-flight (MALDI-TOF) mass spectrometry (MS) to assess purity, size, and correct cleavage of the intein. MALDI-TOF MS was performed using a Bruker Daltonics Microflex mass spectrometer, with  $\beta$ -chain insulin, ubiquitin I, cytochrome C, and  $\beta$ -chain myoglobin (Bruker Daltonics) used as external mass standards for calibration against all subunits produced. Lyophilized standards were resuspended to a final concentration of 50  $\mu$ M in 10  $\mu$ L of 50% (v/v) acetonitrile with 0.1% (v/v) trifluoroacetic acid. The PSI subunits and standards were mixed with 10  $\mu$ L of 60% (v/v) CHCA ( $\alpha$ -cyano-4-hydroxycinnamic acid, Sigma-Aldrich) with 1% (v/v) nitrocellulose. Plates were spotted with 1  $\mu$ L of the mixture and incubated at room temperature overnight in a vacuum desiccator. Spectra were acquired in positive ion mode with reflection, using 300 nitrogen laser pulses/spectrum. The resulting mass/charge data were analyzed using the FindPept program, which is freely accessible on the web at <http://web.expasy.org/findpept/>.

**Western Blotting.** Immobilon PVDF membrane (Millipore) was marked with a number 2 pencil and then activated in 100% methanol for 2 min and soaked in transfer buffer (48 mM Tris, 390 mM glycine, 10% isopropanol) for at least 5 min. Gels were run with prestained markers (EZ-Run prestained, Fischer Scientific, or SeeBlue, Invitrogen). Proteins were transferred from gel to the presoaked PVDF using a Gene transfer apparatus (Idea Scientific) at 24 V for 1.5 h at 4 °C. The blots were removed from the apparatus and incubated in 1 $\times$  TBST (25 mM Tris-HCl, pH 8.0, 137 mM NaCl, 3 mM KCl, 0.1% (v/v) Tween-20) supplemented with 3% (w/v) NFM (nonfat milk) with gentle rocking for 1 h at room temperature with two buffer changes. Next, blots were incubated for 1 h with 1:25000 primary antibody in TBST-NFM. The blots were then washed with TBST-NFM for 3 min with two buffer changes and then incubated with 1:50000 secondary antibody in TBST-NFM for

1 h. The secondary antibody used was a donkey-anti-rabbit horseradish peroxidase conjugate (DAR-HRP, Thermo Scientific). The blots were then washed with TBS for 15 min with two buffer changes. The blots were then dried by blotting on paper towels and incubated with 1 mL total volume of a 1:1 mix of HRP substrate and Luminol (Millipore) for 5 min. The signal was captured with a Chemidoc XRS (Bio-Rad) for 1.5 h, taking images every 15 min. The resulting data was analyzed with Quantity One software, version 4.4 (Bio-Rad), and the bands were quantitated by pixel counting.

**In Vitro PSI Subunit Replacement.** Recombinantly produced ZOBiP–PsaD and/or ZOBiP–PsaE was exchanged with wild-type PsaD and/or PsaE of PSI isolated from Syn 6803 and T.e. in a 10 mL reaction. The final amount of wild-type PSI was 11.3 nmol, and the subunits were present at a 25-fold molar excess. Reactions took place in 1 $\times$  PSI wash buffer supplemented with 0.03%  $\beta$ -DM for 2 h with gentle shaking at room temperature. After exchange, PSI was reisolated over a sucrose gradient, and exchange was verified by SDS-PAGE with Coomassie staining and/or western blotting.

**Subunit, Fd, and PSI Binding to Metal Oxides.** To determine whether ZOBiP enhanced the binding of PsaD/PsaE/PSI to ZnO, a binding assay was performed using ZnO nanoparticles (10–30 nm, US Research Nanomaterials Inc.) or TiO<sub>2</sub> nanoparticles (from the University of Memphis). Briefly, 0.5 mg of ZnO nanoparticles was incubated with 10  $\mu$ g of either WT-PsaD, WT-PsaE, WT-PSI, ZOBiP–PsaD, ZOBiP–PsaE, ZOBiP–PsaD–PSI, or ZOBiP–PsaE in 100  $\mu$ L of 0.1 $\times$  PBS (phosphate buffered saline; 10 mM Na<sub>2</sub>HPO<sub>4</sub>, 2 mM KH<sub>2</sub>PO<sub>4</sub>, 137 mM NaCl, 2.7 mM KCl). Alternatively, 0.5 mg of TiO<sub>2</sub> nanoparticles was incubated with 10  $\mu$ g of either WT-Fd, STB1-Fd, STB2-Fd, or LSTB1-Fd (TOBiP–Fd).<sup>10</sup> The reactions were carried out for 2 h at 4 °C with gentle agitation. ZnO or TiO<sub>2</sub> was pelleted by centrifugation at 1000g for 1 min. The supernatant was collected and is marked as S in Figure 5a,b, and the pellet was washed twice with 100  $\mu$ L of 0.1 $\times$  PBS. Finally, the ZnO or TiO<sub>2</sub> pellet was resuspended in 100  $\mu$ L of 0.1 $\times$  PBS and boiled for 5 min. Following centrifugation, the supernatant was either mixed with 4 $\times$  LSB and SDS-PAGE was performed in the case of PSI subunits (shown as P samples in Figure 5a,b) or quantitated via spectrophotometry if PSI complexes were tested.

**Cross-Linking of PSI and Fd.** PSI and Fd/TOBiP–Fd from T.e. were mixed at a 1:1 molar ratio in 0.1 $\times$  PBS with 0.03% (w/v)  $\beta$ -DM. We used 3.6 nmol of each protein in each reaction with a total volume of 1 mL. The proteins were mixed and incubated on ice for 30 min, and a solution containing 125 mM EDC (1-ethyl-3-(3-(dimethylamino)propyl)carbodiimide hydrochloride, Thermo Scientific) and 250 mM NHS (N-hydroxysuccinimide, Thermo Scientific) was premixed. EDC/NHS was added to final concentrations of 2.5 and 5.0 mM, respectively. The reaction was quenched with addition of 60 °C glycine to a final concentration of 20 mM. The product of this reaction was loaded onto a sucrose gradient, and the PSI-complex was recovered.

**Cyclic Voltammetry.** With various PSI complexes or ferredoxin adsorbed to the surface of the metal oxide ITO glass, the ability of these complexes to donate and receive electrons was assayed by CV (cyclic voltammetry). The  $V_{oc}$  (open circuit potential) was determined for 30 s, and then the potential was set to 0 V (vs  $V_{oc}$ ) and changed at a rate of 50 mV/s to –0.8 V (vs Ag/AgCl) and back to 0 V (vs Ag/AgCl). This scan was performed for five cycles with the sample slide in

200 mM sodium phosphate, pH 6.4. The first three cycles were in the dark, and the next two were illuminated with 1.4 mW/cm<sup>2</sup>, 676 nm band-pass-filtered light.

**Synthesis of Hollow Porous TiO<sub>2</sub> Nanospheres.** The TiO<sub>2</sub> nanospheres (NS) were synthesized via a hydrothermal method in the presence of glucose: 7.5 g of glucose and 1.5 g of (NH<sub>4</sub>)<sub>2</sub>TiF<sub>6</sub> were dissolved in 40 and 20 mL of distilled water, respectively. The two solutions were mixed by stirring for 30 min. The resulting solution was poured into a Teflon-coated stainless steel autoclave (80 mL). The autoclave was placed into the furnace at 180 °C for 24 h. After the autoclave was cooled naturally to room temperature, the resultant product, semi-crystalline precipitates of TiO<sub>2</sub> embedded in the caramelized glucose, was centrifuged for collection. The as synthesized precipitates were washed at least five times with distilled water and ethyl alcohol. The resulting precipitates were then dried at 80 °C for 15 h. The dried precipitates were calcined at either 550 or 700 °C for 3 h to obtain highly crystalline and porous anatase TiO<sub>2</sub> nanospheres,<sup>25,26</sup> as confirmed by X-ray diffraction and scanning electron microscopy.

## ■ ASSOCIATED CONTENT

### ■ Supporting Information

The Supporting Information is available free of charge on the ACS Publications website at DOI: 10.1021/acs.bioconjchem.5b00374.

Different TiO<sub>2</sub> nanoparticles and nanospheres observed by EM and the effects of various additives on TOBiP–Fd retention by TiO<sub>2</sub> (PDF).

## ■ AUTHOR INFORMATION

### Corresponding Author

\*E-mail: bbruce@utk.edu.

### Notes

The authors declare no competing financial interest.

## ■ ACKNOWLEDGMENTS

B.D.B. and S.R.M. acknowledge support from TN-SCORE, a multidisciplinary research program sponsored by NSF-EPSCoR (EPS-1004083). R.F.S., T.Z., and B.D.B. acknowledge support from the UTK BCMB Department and from the Gibson Family Foundation. R.F.S. was supported as an IGERT Fellow from the National Science Foundation IGERT program (DGE-0801470). B.D.B., D.R.B., and C.A.L. also acknowledge support from the Directors Strategic Initiative, “Understanding Photosystem I as a Biomolecular Reactor for Energy Conversion” at the Army Research Laboratory, Adelphi, MD (ARL contract no. W911NF-11-2-0029). We would like to thank Dr. John Dunlap for help with electron microscopy. We also appreciate the support and feedback provided by Ridge Carter, Khoa Nguyen, and Kristen Holbrook while conducting this research.

## ■ ABBREVIATIONS

DSSC, dye-sensitized solar cell; Fd, ferredoxin; MOBiP, metal oxide binding peptide; PSI, Photosystem I; TOBiP, titanium oxide binding peptide; ZOBiP, zinc oxide binding peptide

## ■ REFERENCES

(1) Blankenship, R. E., and Hartman, H. (1998) The origin and evolution of oxygenic photosynthesis. *Trends Biochem. Sci.* 23 (3), 94–7.

(2) Rochaix, J. D. (2011) Regulation of photosynthetic electron transport. *Biochim. Biophys. Acta, Bioenerg.* 1807 (3), 375–83.

(3) Nguyen, K., and Bruce, B. D. (2014) Growing green electricity: progress and strategies for use of Photosystem I for sustainable photovoltaic energy conversion. *Biochim. Biophys. Acta, Bioenerg.* 1837 (9), 1553–1566.

(4) Kim, Y., Shin, D., Chang, W. J., Jang, H. L., Lee, C. W., Lee, H.-E., and Nam, K. T. (2015) Hydrogen evolution: hybrid Z-scheme using Photosystem I and BiVO<sub>4</sub> for hydrogen production. *Adv. Funct. Mater.* 25 (16), 2345–2345.

(5) Iwuchukwu, I. J., Vaughn, M., Myers, N., O'Neill, H., Frymier, P., and Bruce, B. D. (2010) Self-organized photosynthetic nanoparticle for cell-free hydrogen production. *Nat. Nanotechnol.* 5 (1), 73–9.

(6) Ciesielski, P. N., Hijazi, F. M., Scott, A. M., Faulkner, C. J., Beard, L., Emmett, K., Rosenthal, S. J., Cliffl, D., and Kane Jennings, G. (2010) Photosystem I-based biohybrid photoelectrochemical cells. *Bioresour. Technol.* 101 (9), 3047–53.

(7) Merchant, S., and Sawaya, M. R. (2005) The light reactions: a guide to recent acquisitions for the picture gallery. *Plant Cell* 17 (3), 648–63.

(8) Zanetti, G., and Merati, G. (1987) Interaction between photosystem I and ferredoxin. Identification by chemical cross-linking of the polypeptide which binds ferredoxin. *Eur. J. Biochem.* 169 (1), 143–6.

(9) Kjaergaard, K., Sorensen, J. K., Schembri, M. A., and Klemm, P. (2000) Sequestration of zinc oxide by fibrous designer chelators. *Applied and environmental microbiology* 66 (1), 10–4.

(10) Chen, H., Su, X., Neoh, K. G., and Choe, W. S. (2008) Probing the interaction between peptides and metal oxides using point mutants of a TiO<sub>2</sub>-binding peptide. *Langmuir* 24 (13), 6852–7.

(11) Macwan, D. P., Dave, P. N., and Chaturvedi, S. (2011) A review on nano-TiO<sub>2</sub> sol-gel type synthesis and its applications. *J. Mater. Sci.* 46 (11), 3669–3686.

(12) Mathew, S., Yella, A., Gao, P., Humphry-Baker, R., Curchod, B. F., Ashari-Astani, N., Tavernelli, I., Rothlisberger, U., Nazeeruddin, M. K., and Gratzel, M. (2014) Dye-sensitized solar cells with 13% efficiency achieved through the molecular engineering of porphyrin sensitizers. *Nat. Chem.* 6 (3), 242–7.

(13) Chang, H., Hsu, C.-M., Kao, P.-K., Yang, Y.-J., Hsu, C.-C., Cheng, I. C., and Chen, J.-Z. (2014) Dye-sensitized solar cells with nanoporous TiO<sub>2</sub> photoanodes sintered by N<sub>2</sub> and air atmospheric pressure plasma jets with/without air-quenching. *J. Power Sources* 251 (0), 215–221.

(14) Jordan, P., Fromme, P., Witt, H. T., Klukas, O., Saenger, W., and Krauss, N. (2001) Three-dimensional structure of cyanobacterial photosystem I at 2.5 Å resolution. *Nature* 411 (6840), 909–17.

(15) Cashman, D. J., Zhu, T., Simmerman, R. F., Scott, C., Bruce, B. D., and Baudry, J. (2014) Molecular interactions between photosystem I and ferredoxin: an integrated energy frustration and experimental model. *J. Mol. Recognit.* 27 (10), 597–608.

(16) Hall, D. O., Cammack, R., and Rao, K. K. (1973) The plant ferredoxins and their relationship to the evolution of ferredoxins from primitive life. *Pure Appl. Chem.* 34, 553.

(17) Minai, L., Fish, A., Darash-Yahana, M., Verchovsky, L., and Nechushtai, R. (2001) The assembly of the PsdA subunit into the membranous photosystem I complex occurs via an exchange mechanism. *Biochemistry* 40 (43), 12754–60.

(18) Lushy, A., Verchovsky, L., and Nechushtai, R. (2002) The stable assembly of newly synthesized PsdA into the photosystem I complex occurring via the exchange mechanism is facilitated by electrostatic interactions. *Biochemistry* 41 (37), 11192–9.

(19) Mershin, A., Matsumoto, K., Kaiser, L., Yu, D., Vaughn, M., Nazeeruddin, M. K., Bruce, B. D., Graetzel, M., and Zhang, S. (2012) Self-assembled photosystem-I biophotovoltaics on nanostructured TiO<sub>2</sub> and ZnO. *Sci. Rep.* 2, 234.

(20) Kim, Y., Shin, S. A., Lee, J., Yang, K. D., and Nam, K. T. (2014) Hybrid system of semiconductor and photosynthetic protein. *Nanotechnology* 25 (34), 342001.



- (21) Sreerama, N., Venyaminov, S. Y., and Woody, R. W. (2000) Estimation of protein secondary structure from circular dichroism spectra: inclusion of denatured proteins with native proteins in the analysis. *Anal. Biochem.* 287 (2), 243–51.
- (22) Sreerama, N., Venyaminov, S. Y., and Woody, R. W. (1999) Estimation of the number of alpha-helical and beta-strand segments in proteins using circular dichroism spectroscopy. *Protein Sci.* 8 (2), 370–80.
- (23) Provencher, S. W., and Glockner, J. (1981) Estimation of globular protein secondary structure from circular dichroism. *Biochemistry* 20 (1), 33–7.
- (24) Johnson, W. C. (1999) Analyzing protein circular dichroism spectra for accurate secondary structures. *Proteins: Struct., Funct., Genet.* 35 (3), 307–12.
- (25) Wang, H. Q., Wu, Z. B., and Liu, Y. (2009) A simple two-step template approach for preparing carbon-doped mesoporous TiO<sub>2</sub> hollow microspheres. *J. Phys. Chem. C* 113 (30), 13317–13324.
- (26) Liu, G., Yan, X. X., Chen, Z. G., Wang, X. W., Wang, L. Z., Lu, G. Q., and Cheng, H. M. (2009) Synthesis of rutile-anatase core-shell structured TiO<sub>2</sub> for photocatalysis. *J. Mater. Chem.* 19 (36), 6590–6596.